Advances in Radiation Oncology (2020) **5**, 1-16

advances
in radiation oncology

www.advancesradonc.org

Critical Review

Technical Principles of Dual-Energy Cone Beam Computed Tomography and Clinical Applications for Radiation Therapy

Shailaja Sajja, MASc,[a,b] Young Lee, PhD,[c] Markus Eriksson, MSc,[d] Håkan Nordström, PhD,[d] Arjun Sahgal, MD,[c] Masoud Hashemi, PhD,[a] James G. Mainprize, PhD,[a] and Mark Ruschin, PhD[c,*]

[a]Sunnybrook Research Institute, Toronto, Ontario, Canada; [b]QIPCM Imaging Core Lab, Techna Institute, Toronto, Ontario, Canada; [c]Department of Radiation Oncology, Sunnybrook Health Sciences Centre, University of Toronto, Toronto, Ontario, Canada; and [d]Elekta Instrument AB, Stockholm, Sweden

Received 25 January 2019; revised 21 May 2019; accepted 20 July 2019

Abstract

Purpose: Medical imaging is an indispensable tool in radiotherapy for dose planning, image guidance and treatment monitoring. Cone beam CT (CBCT) is a low dose imaging technique with high spatial resolution capability as a direct by-product of using flat-panel detectors. However, certain issues such as x-ray scatter, beam hardening and other artifacts limit its utility to the verification of patient positioning using image-guided radiotherapy.

Methods and Materials: Dual-energy (DE)-CBCT has recently demonstrated promise as an improved tool for tumor visualization in benchtop applications. It has the potential to improve soft-tissue contrast and reduce artifacts caused by beam hardening and metal. In this review, the practical aspects of developing a DE-CBCT based clinical and technical workflow are presented based on existing DE-CBCT literature and concepts adapted from the well-established library of work in DE-CT. Furthermore, the potential applications of DE-CBCT on its future role in radiotherapy are discussed.

Results and Conclusions: Based on current literature and an investigation of future applications, there is a clear potential for DE-CBCT technologies to be incorporated into radiotherapy. The applications of DE-CBCT include (but are not limited to): adaptive radiotherapy, brachytherapy, proton therapy, radiomics and theranostics.

Sources of support: This work had no specific funding.

Disclosures: Dr Sahgal has received honoraria for educational seminars and receives a research grant from Elekta Instrument AB. Dr Ruschin is the coinventor of and owns associated intellectual property specific to the image-guidance system on the Gamma Knife Icon. Dr James Mainprize is supported by grants from GE health care. Drs Eriksson and Nordstrom are employees of Elekta Instrument AB, otherwise, the authors have no conflicts of interest to declare.

* Corresponding author: Mark Ruschin, PhD; E-mail: Mark.Ruschin@sunnybrook.ca

https://doi.org/10.1016/j.adro.2019.07.013

Introduction

Cone beam computed tomography (CBCT) has become the standard of practice in radiation therapy verification imaging[1,2] and has facilitated the safe adoption around the world of stereotactic body radiation therapy (SBRT) with reduced treatment margins. A radiation therapy department could potentially produce thousands of CBCT images over the course of a year. It would be interesting if these images could be used to obtain specific information in addition to bony anatomy for verification of patient setup.

However, CBCT is challenged by image nonuniformity caused by x-ray scatter and artifacts such as beam hardening (BH), which result in reduced soft-tissue visibility and loss in CT number accuracy.[3] CBCT has therefore primarily been a bony anatomy imaging modality. Although some soft tissue can be differentiated (such as bladder volumes within the pelvic soft tissue), direct tumor visualization is only possible where there is sufficient contrast between the tumor and the background tissue such as between a solid tumor and low-density lung.[2] Post treatment, the CBCT images are archived (often for legal purposes) and rarely accessed again. Furthermore, adaptive radiation therapy to compensate for changes in patient anatomy is challenging because CBCT artifacts limit the accuracy of dose calculations necessitating a comprehensive artifact correction.[4] Given the widespread use of CBCT, different methods to enhance visualization, improve CT number accuracy, and potentially quantify tumor changes by reduction of scatter and BH are being investigated.[5-7]

One approach toward realizing quantitative imaging, while addressing enhanced tissue visualization in CBCT, is the concept of dual energy imaging. Duel energy (DE) CT can provide quantitative information regarding the inherent materials in the image and also differentiate materials. This has attracted attention in recent years in diagnostic radiology[8-13] and in its potential role in radiation therapy planning and treatment delivery.[14] The present review article focuses on the potential of DE using CBCT (ie, DE-CBCT) because CBCT arising from daily image guidance accounts for a majority of CT scans acquired in radiation therapy.

The review is organized as follows: a description of the physical basis of DE-CBCT and various image acquisition techniques for acquiring DE-based volumetric imaging, reconstruction options, and an overview of radiation therapy-based applications.

Physics and Technical Aspects of Dual-Energy CBCT Imaging

Background

The use of DE to improve radiologic contrast was first described by Jacobson et al in 1958[15] followed by Mistretta et al[16] and Alvarez and MacOvski[17] in the mid-1970s. With the introduction of new large area flat-panel detectors (FPDs)[18] that provide high dose efficiency and rapid projection readout, there has been renewed interest in using DE imaging.

Generic requirements for DE imaging

In the diagnostic x-ray energy range, photoelectric effect and Compton scatter contribute to the attenuation coefficient of a material. The relative contributions of Compton scatter and photoelectric effect components vary with energy. This variation helps in materials differentiation.

With the exception of a few systems using synchrotron radiation as an energy selective source,[19,20] most practical DE systems rely on x-ray sources that generate polyenergetic spectra. For DE imaging to be feasible, sources providing x-rays with at least 2 different energy ranges are typically required. It is beneficial to maximize the separation between the spectra.[21] X-ray tube voltages lower than 70 kVp have limited practical use because the majority of photons is absorbed by the human body[22] with some exceptions such as in mammography and dental applications. Typical diagnostic x-ray imaging systems are not capable of emitting energies greater than 140 kVp[22] because the tubes are made compact, which limits heat capacity.

With the exception of photon counting detectors[23,24] (described in this article), the majority of commercial detectors operate as energy integrators, ie, the signal intensity at a given detector element corresponds to the integrated energy fluence of the photons during the readout interval.

Available technologies in DE-volumetric (CT/CBCT) imaging

The generic CBCT workflow is illustrated in Figure 1. Based on the approaches commonly presented for DE-CT and recent works in DE-CBCT, there are different technologies currently available for the acquisition of DE image sequences. Although there may be other approaches for DE-CBCT, the present review has focused on the main technologies represented in the literature.

X-ray source selection

As illustrated in Figure 1, the first step in the image acquisition workflow involves the emission of x-ray photons from the tube. It is possible to acquire high-energy (HE) and low-energy (LE) x-ray projections by modifications at the source or tube step. Two such methods are discussed here.

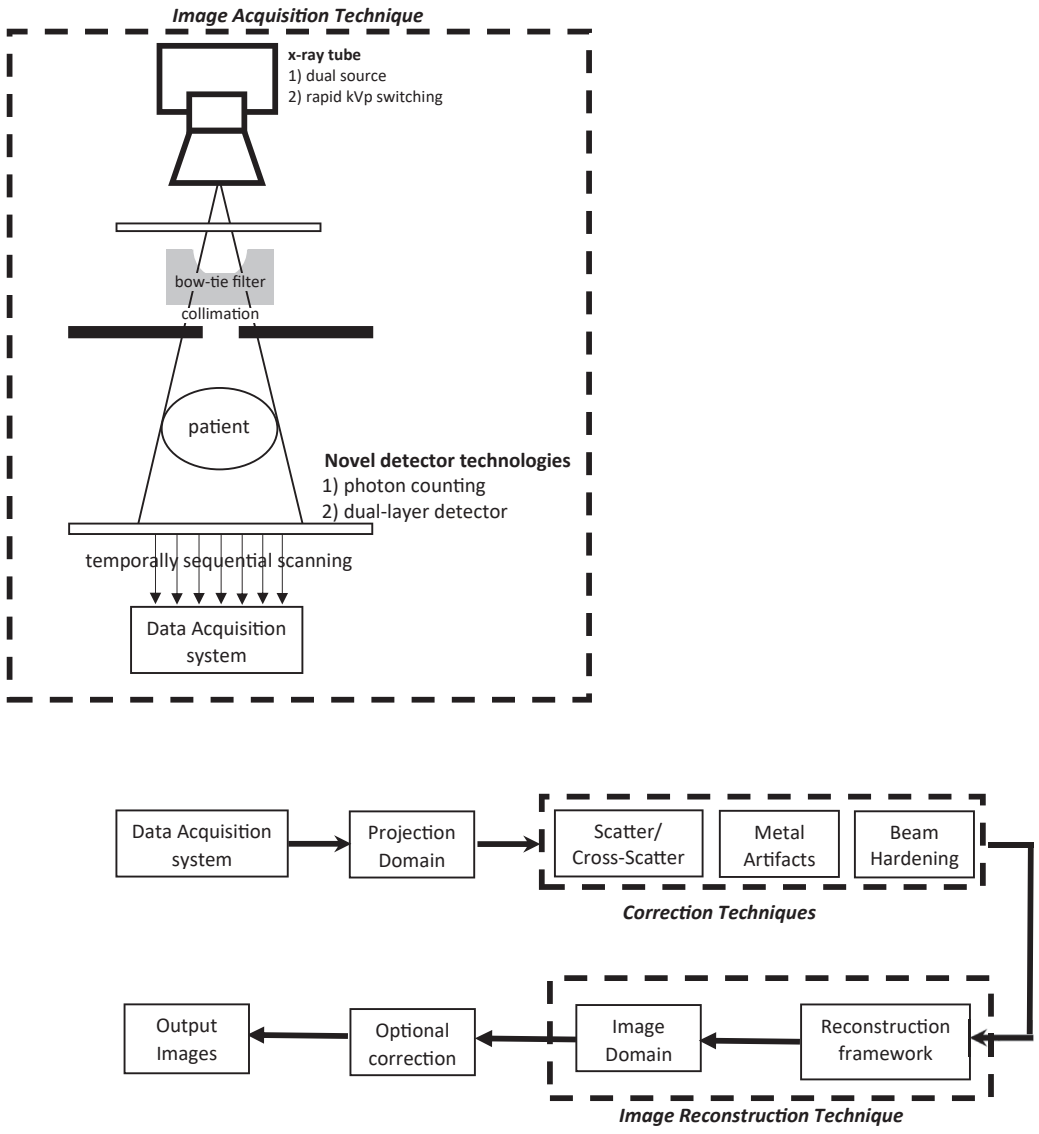

Figure 1 The Cone beam computed tomography imaging chain illustrating the various DE imaging acquisition options. X-ray tube based: (1) dual source, (2) rapid kVp switching. Novel detector based: (1) dual-layer detector and (2) photon counting. Also, by acquiring 2 consecutive cone beam computed tomographic scans, temporally sequential scanning is possible. The workflow from data acquisition to the formation of output images is illustrated.

Dual-source and multisource

Dual or multisource techniques generally involve x-ray sources and detectors placed orthogonal to each other.[25-27] In addition, a filter can be used with the HE source to harden the beam and increase spectral separation. Reconstruction is done separately for 2 data sets. Because the x-ray sources are orthogonal to each other, postprocessing is required to align the HE and LE projections to each other.

The strengths of this technique are that the HE and LE images are acquired with only one rotation using established x-ray sources and detectors. Existing techniques can be used to reconstruct the HE and LE images separately. The tube current and filtration for each of the 2 sources can be adjusted independently. As the spectral overlap can be minimized, the contrast-to-noise ratios (CNR) in the material specific images are improved.[28]

The challenges are that specialized hardware[8] are required for acquisition (2 sources) and specialized software is required for scatter correction.[8] An additional form of scatter known as cross scatter[29] is observed, in which a photon from one source is scattered and detected by the orthogonal detector. Cross scatter requires specialized scatter correction algorithms.[30,31] Alternatively an interleaved configuration to reduce cross-scatter was presented in Giles et al,[29] such that each source acquires projections alternatively instead of simultaneously.

The dual-source or multisource techniques presented in the DE-CBCT literature can be broadly classified into kV-kV, kV-MV, and multisource dual energy techniques.

kV-kV dual source

This indicates the usage of 2 kV sources for acquiring the HE and LE images. Li et al[32,33] used an in-house benchtop system consisting of 2 orthogonally placed FPDs and 2 conventional x-ray tubes sharing the same rotational axis. One FPD acquired projections corresponding to a 0- to 90-degree angular range and the other FPD acquired projections from a nonoverlapping (90- to 200-degree) angular range. The results of the work supported the further development of dual source CBCT system. There is a reduction in scan time translating clinically into reduced motion artifacts. Additional work by the same group looked at scatter reduction by usage of grids attached to both x-ray sources.[30]

kV-MV dual source

As modern linear accelerators are designed with a kV and a MV panel, a series of works have investigated the possibilities of kV-MV imaging using dual source. This work was motivated by the rationale that MV beams undergo comparatively lesser attenuation then kV beams hence is potentially capable of penetrating through larger objects accompanied by a potential reduction in metal artifacts.[34] Blessing et al[35] and Wertz et al[36] investigated the potential for kV-MV imaging using a histogram adaptation technique to map the projections from the MV range to kV range.

Recently, a benchtop system was used to acquire an orthogonal set of projections with energies in the kV and MV range, respectively.[34] The overall workflow for decomposition and acquisition is shown in Figure 2. One FPD acquired projections corresponding to a 0- to 100-degree angular range and the other FPD acquired projections from a 90- to 200-degree angular range. This allows for a 10-degree overlap between the kV and MV projections, facilitating the creation of virtual monochromatic projections (VMP), a concept which will be introduced further in the article. The challenges of the technique include using a linear approximation to convert kV/MV projections into VMP, hence some artifacts persist owing to the imperfect conversion. Second, because MV beams are higher than 1.02 MeV, there is a small possibility of pair production.[34] Also, because the projections were mapped onto one coordinate system during the reconstruction process, the misalignment between the kV and MV isocenters and tilt of detector can lead to artifacts.[34]

Multisource

Zbijewski et al[37] reported on a multisource system. It is a research prototype similar to the commercially available Onsight 3D Extremity System (Carestream Health, Rochester, NY). It consists of a scanner with 3 x-ray sources distributed along the longitudinal direction.

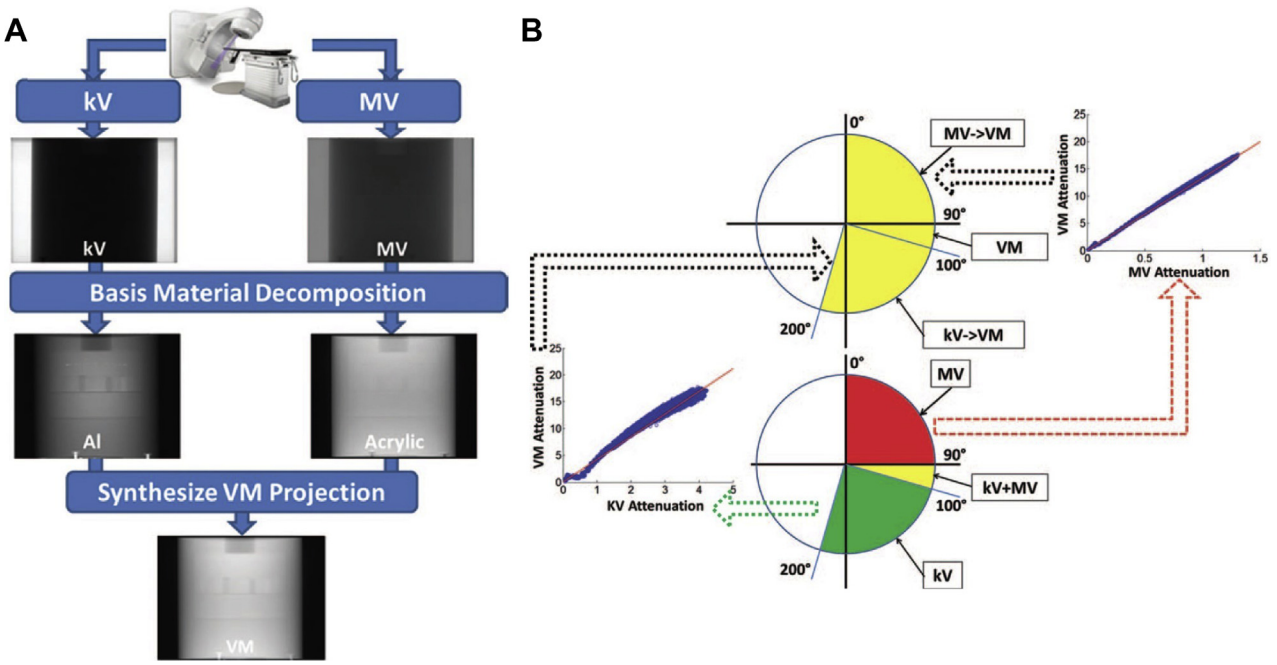

Figure 2 Technique for virtual monochromatic imaging using kV-MV imaging. (A) Process for the synthesis of virtual monochromatic projections from kV and MV. (B) A linear conversion function for conversion of MV and kV projections to VMP was calculated at overlap angles. The same function was used to create approximate VMP at nonoverlap angles. Adapted with permission from reference Li et al.[34]

Both peripheral sources exposed 180 HE projections each and the central source exposed 360 LE projections. This acquisition strategy provides an extension of the field-of-view, reduction of the cone beam artifacts and faster acquisition of DE-CBCT projections.[37] Data from each HE source were reconstructed separately and averaged. The clinical application was the detection and visualization of bone marrow edema, which is usually challenging to visualize using CBCT owing to the overlying trabecular structure.

Rapid kVp switching

For rapid kVp switching as seen in DE-CT,[22,38-40] the hardware associated with the source or tube and control software associated with the generator is modified, enabling it to follow pulsed patterns and produce HE and LE exposures at each near-identical detector locations. The strengths are minimization of motion artifacts and reduction in acquisition time.

The challenges are that the system must possess the ability to enable rapid kVp rise and fall hence necessitating a fast switching generator. Also, detector primary and secondary decay can cause blurring between views.[39]

kVp switching has been investigated in microCT systems,[41] which is similar to CBCT systems using a 2-dimensional detector. The dimensions of microCTs restrict their usage to preclinical research. Min et al[41] studied a novel technique based on a total-variation minimization algorithm using 2 phantoms and mouse subjects.

Detector-based techniques

It is also possible to acquire DE acquisitions using an energy-integrating FPD and also with novel detector technologies. Two such technologies are dual-layer detector and photon-counting detectors (PCDs).

FPD detector

It is possible to use energy-integrating FPDs for DE-CBCT. A commonly deployed technique for DE-CBCT imaging is temporally sequential scanning. With temporally sequential scanning, 2 consecutive CBCT scans at HE and LE are acquired. The strength of this technique is that no modification is needed to the existing scanner setup for image acquisition. However, this technique is challenged by the increased acquisition time, which translates to blurring and motion artifacts resulting from patient or specific organ motion.

Most of the DE-CBCT research has used a sequential scanning technique.[42-45] Traditional reconstruction techniques can be used for image formation.

Dual-layer detector

In the context of DE-CT, this technique uses a detector typically consisting of 2 stacked layers. The image acquisition process consists of acquiring a single scan at high kVp. The material composition of the 2 layers (eg, ZnSe or CsI in the top layer and Gd_2O_2S in the bottom layer)[22] is such that the top layer absorbs majority of the LE photons and the bottom layer absorbs the remaining HE photons.[46] The strengths are that because the spectral energy separation occurs within the detection system as opposed to different sources or sequential scans, there is no time lag or spatial shifts between the HE and LE projections; and also the need to redundantly expose materials or clinical subjects with HE and LE separately is removed.[46] Because the acquisitions are acquired via single scan, no additional imaging dose is delivered to the patient when using dual-layer detectors. Also, additional processing can occur at any time after the acquisition (such as in a future analysis) as the data are already there.

The challenges are there is high overlap between HE and LE spectra and differing noise levels between the resultant HE and LE images. There are series of works with the usage of dual-layer detectors in radiographic applications.[47,48] There is no published data on kV CBCT dual-layer detector systems. However, a series of works[49-57] have reported the development of multilayer imagers (MLI) for MV CBCT imaging. These works present various aspects such as the 1) framework for analysis and design of MLIs,[50] 2) a comprehensive computational model for MLI optimization,[52] 3) task specific optimization[53] such as bone separation,[54] and 4) configurations to achieve superresolution imaging[55] and improved image quality by stacking and shifting multiple layers relatively to each other.

Photon Counting Detectors (PCDs)

PCDs,[58-60] a recent development in the field of x-ray-based detector research, allow spectral measurements at different and relatively independent energies by use of a technology comprised of high-speed, typically solid state, radiation sensors combined with fast readout application-specific integrated circuits, which can process individual photons.[61,62] Such detectors are also referred to as quantum counting detectors or energy-resolved PCDs. PCDs are capable of counting photons based on the detected energies within multiple energy thresholds.[63] This is illustrated in Figure 3.

The strengths are the potentially improved CNR ratio and reduction of acquisition time and motion artifacts due to a single acquisition.[60] Similar to dual-layer detectors, in PCDs no additional imaging dose is delivered to the

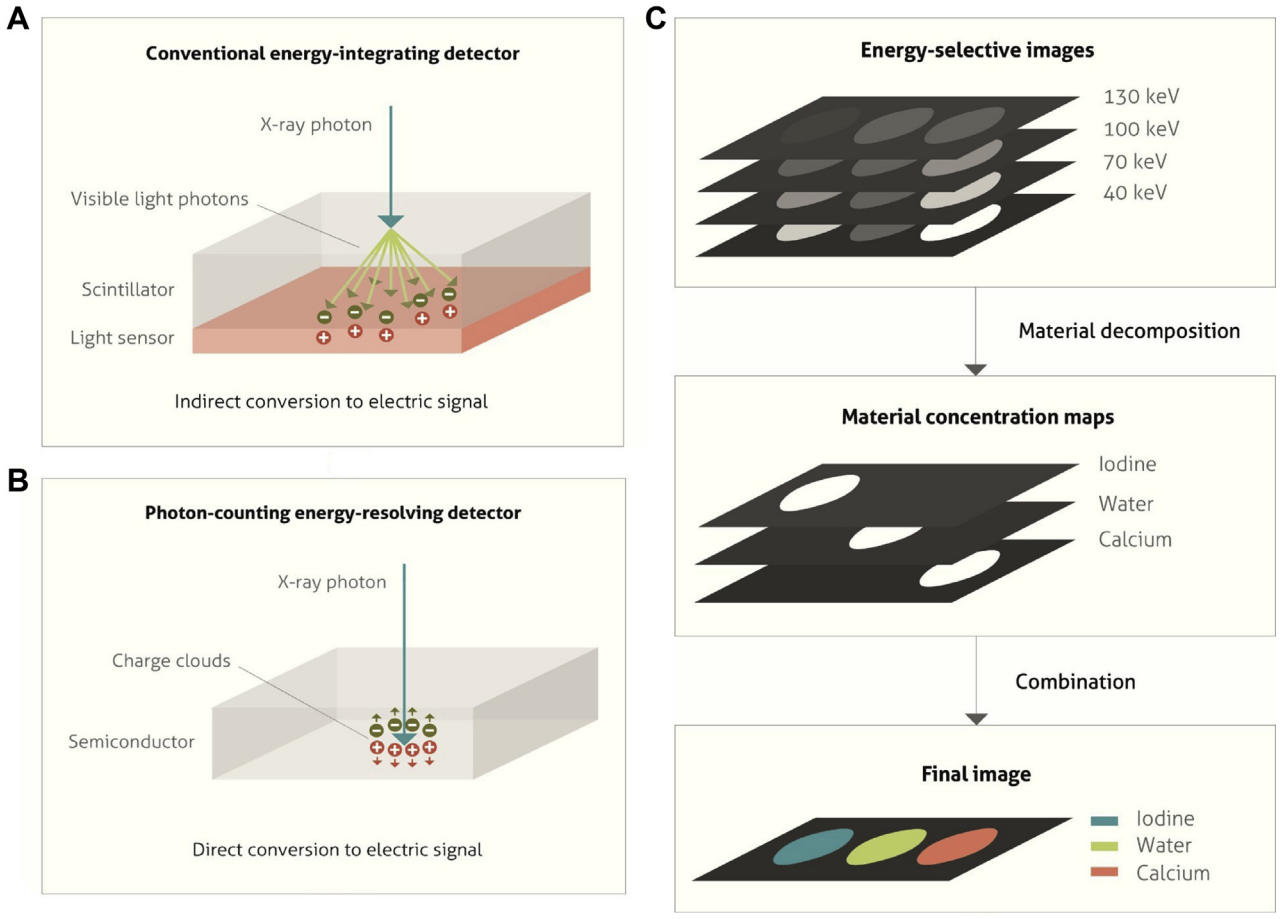

Figure 3 Principle of photon counting detector (PCD) for spectral separation. (A) The depiction of the process of conversion of an incident x-ray photon into shower of visible light photons in the scintillator followed by generation of positive and negative electrical charges on hitting the underlying light sensor in an energy-integrating detector. (B) In PCD, the semiconductor material absorbs the x-ray photon hence generating positive and negative charges. An electrical signal is generated owing to the influence of a strong electric field, which pulls the positive and negative charges in opposite directions. (C) Two-stage material decomposition involving formation of energy-selective images from the number of registered counts in each energy bin, followed by the formation of material concentration maps. Adapted with permission from reference Willemink et al.[119]

patient and further processing of the data can be conducted at any future time.

The main challenges include the requirement of sophisticated detectors and electronics resulting in increased costs. Furthermore, ring artifacts tend to occur due to detector sensitivity variation arising from the energy dependence and spectral distortions caused by charge sharing. Charge sharing[58] occurs when incorrect energies are recorded as the energy from a photon incident on one detector pixel simultaneously results in a count in the corresponding pixel and neighboring pixels. Currently techniques are being investigated to reduce charge sharing effects.[58]

Use of PCDs was investigated in a dual-energy C-arm angiographic system.[59] A phantom study demonstrated the ability to perform material decomposition and the CNR metrics obtained using PCDs were comparable to those obtained using a standard detector.[59]

Factors for optimization of DE performance

The various image acquisition technique factors, which would affect the performance of DE imaging, are presented.

Contrast or noncontrast imaging in conjunction with DE imaging: The use of exogenous contrast agents helps in differentiating structures with otherwise similar attenuation behavior and material composition. For instance, it can be used to enhance vessels, which do not contain calcium to assess the carotid and vertebral arteries in the skull base and the cervical spine.[64] For neuroimaging applications, brain parenchyma and most types of tumors have similar x-ray attenuation behavior; hence the intravenous administration of contrast, often iodine, is typically used to enhance visibility. DE-CT imaging can be used for separation of iodine.[11,65]

Energy selection: Energy selection is dictated by tube capabilities, body part thickness (penetration), task (eg,

soft tissue vs bone, contrast agent vs background). The choice of HE or LE affect the performance of resultant DE images.[46,47] In general, the choices would apply to DE-CBCT imaging as well.[21]

Dose allocation: The reconstructed images are generally more sensitive to the noise in the HE image,[66] although too little dose allocated to the LE can lead to photon starvation. Hence the ratio of the allocation of the dose between the HE and LE is important. In one study,[67] it was found that more dose from the HE scan relative to the LE scan yielded improved image quality.

Choice of filtration: As maximal separation of the spectra is beneficial for optimal performance of the DE imaging; a filter is typically made of high atomic number materials. When the x-ray beam passes through the filter, LE photons are preferentially absorbed, hardening the beam. For DE imaging, 3 configurations are possible with regard to filtration:

(1) No filtration.
(2) Fixed filtration: same filtration is added to the HE and LE beams.
(3) Differential filtration: Filtration is different between the HE and LE beams.

Differential filtration would result in the best separation of the HE and LE beams and minimizes the wasted radiation. For one DE radiography system, (5 mm Al + 0.3 mm Cu) for LE and (0.3 mm Cu + 0.5 mm Ag) for HE was identified as near optimal.[66] In particular, the materials with atomic numbers from 25 to 50 were found to provide optimal filtration. An investigation of optimal filtration for DE-CBCT has not been carried out so far.[67] For DE-CT, 7 different single element filter materials were found to have similar performance. However, Sn filtration was chosen due to its low cost and ease of preparation.[26] From a practical perspective it could be challenging to place such additional filtration layers to an existing commercial system. The complexity of this modification would depend of the manufacturer of the LINAC system.

Interscan time (IST): This is the period between the same projection number corresponding to the HE and LE sequences and is dependent on the image acquisition technology. When detector-based techniques such as dual-layer or PCDs are used or the dual source technique is used, IST is 0. For temporally sequential scans, IST is approximately equal to a single scan time. IST is particularly important in clinical applications as subject motion can result. For rapid-kV switching, the approximate IST is equal to the time between 2 adjacent projection angles which comprise of the time required to transition between energies and the detector readout time. For optimal performance, it is beneficial to have an IST as small as possible.

Reconstruction–decomposition workflow (image vs projection-domain decomposition)

After the acquisition of HE and LE scans, the next steps are decomposition and reconstruction of data. In addition, artifact correction is an important part of the workflow to improve the quality of images. If decomposition is performed before reconstruction and virtual monochromatic projections are created, certain artifacts such as BH and relevant metal artifacts[42,68] are minimized.

Prereconstruction techniques

These are techniques where decomposition into basis materials is performed before reconstruction, also referred to in literature as projection-domain techniques or raw-domain techniques. Projection-domain techniques are suitable in cases where there is data consistency between HE and LE projections. These techniques work well when the HE and LE projections are acquired under the same conditions: (1) patient positioning, (2) points in the breathing-cardiac cycle or gastric cycle, and (3) same corresponding angles. Preference for this technique is based on the image acquisition technique, the organ being imaged and the disease state of the organ as some diseases in certain organs such as the heart are accompanied by increased motion.

Prereconstruction techniques are primarily used in combination with rapid kVp switching. For PCDs, it is possible to use both projection-domain and image-domain techniques for DE decomposition. However, image-domain techniques are preferable as projection-domain techniques require rigorous calibration of the basis material functions and energy response of the imaging system.[61]

Projection-domain techniques typically involve a calibration step[69] where phantoms composed of materials similar in radiologic properties to soft tissue and bones (eg, acrylic and aluminum) are used to capture the material attenuation properties and behavior of the system. The information is used to decompose the projections into the basis materials. This information further allows for the construction of VMPs. Metal and BH artifacts are caused due to the polychromatic nature of the x-ray beam, hence by the use of VMPs, these artifacts can be reduced.

In cases where it is imperative to use this technique despite the likelihood of occurrence of motion artifacts (for instance in temporally sequential scans), the development of robust registration techniques adapted from existing techniques[70] is highly beneficial.

Virtual monochromatic images (VMIs) are obtained by the decomposition of the HE and LE images in the projection-domain in basis materials followed by their combination weighted by their attenuation coefficients as

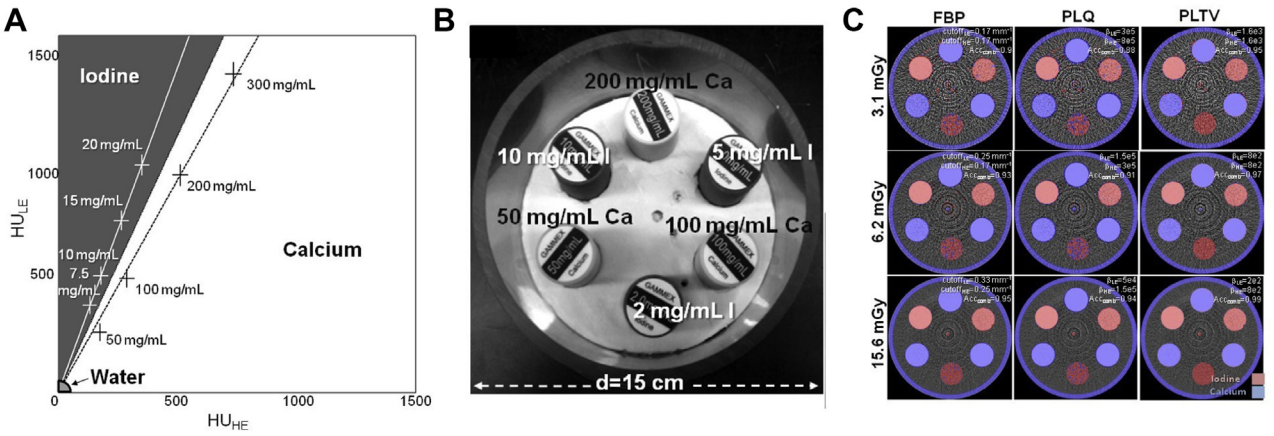

Figure 4 Technique used for dual-energy cone beam computed tomography calibration and material classification. (A) Energy map. (B) Illustration of the phantom used with various iodine and calcium inserts. (C) Dual-energy cone beam computed tomography classification with Iodine is shown as a red overlay and calcium as a blue overlay on composite filtered back projection, quadratic penalty, and quadratic penalty and total-variation penalty (different reconstruction algorithms) images for each dose. Adapted with permission from reference Zbijewski et al.[43]

VMPs at a given energy and subsequently reconstructed as VMIs. Hypothetically, VMIs are representative of what the image would look like if the acquisition was performed using a monochromatic x-ray beam.

Postreconstruction techniques

These techniques where decomposition follows reconstruction, also referred to in literature as image-domain techniques, are suited in scenarios where the corresponding HE and LE projections are acquired at differing corresponding angles or under different conditions. Hence these techniques are more widely applicable compared with projection-domain techniques. However, an additional artifact correction step[71] is needed to correct BH and reduce metal artifacts.

A separation or classification technique is often used for DE decomposition whereby the HE and LE images are mapped into a plane created from the HU values of the LE images versus the HU values of the HE images. This is known as the energy map.[46] A line drawn across the map could potentially classify the image regions into one material or the other, based on whether the values lie above or below the drawn line on the map. More sophisticated advances to this technique exist, such as vectorial or probability separation.[46] In the vector technique, the HU value of each voxel can be seen as a vector summation of the 2 vectors along the corresponding material axes in the energy map. Similarly, probabilistic separation techniques rely on a statistical model for material separation. This is particularly relevant in cases where there is a high likelihood of noise which can affect the integrity of the spectral information.[46] The separation of iodine and calcium using this technique was done in Zbijewski et al,[43] and the performance of different reconstruction techniques, namely filtered back projection, and 2 variants of penalized likelihood (PL) reconstruction: quadratic penalty and total-variation penalty were compared (Fig 4). Quadratic penalty and total-variation penalty performed overall better than filtered back projection and quadratic penalty.[43]

Linearly mixed images, also referred to in literature as linearly-blended images or weighted-average images, result from the linear combination of the reconstructed HE and LE images in different proportions. Some works[72,73] also explore nonlinear combination of the images.

Current and Potential Applications

Improved image quality

Tumor visualization, delineation, and tracking

Tumor (target) localization is extremely important in SBRT and stereotactic radiosurgery where high radiation doses are delivered in a limited number of treatment fractions, resulting in a low tolerance for localization uncertainties.[2] Although image guidance using CBCT has been widely used to verify patient setup during the past 2 decades, the technique is limited by artifacts that can in part be mitigated by DE-CBCT. Additionally, DE-CBCT in conjunction with contrast injection has the potential for true tumor-guided radiation therapy. This would, however, be a rate-limiting step in a busy clinic and may be preferable to use in treatment techniques involving limited number of fractions such as stereotactic radiosurgery or SBRT treatments.

DE-CT has been shown to improve tumor and normal tissue visualization[74,75]; however, there is no currently

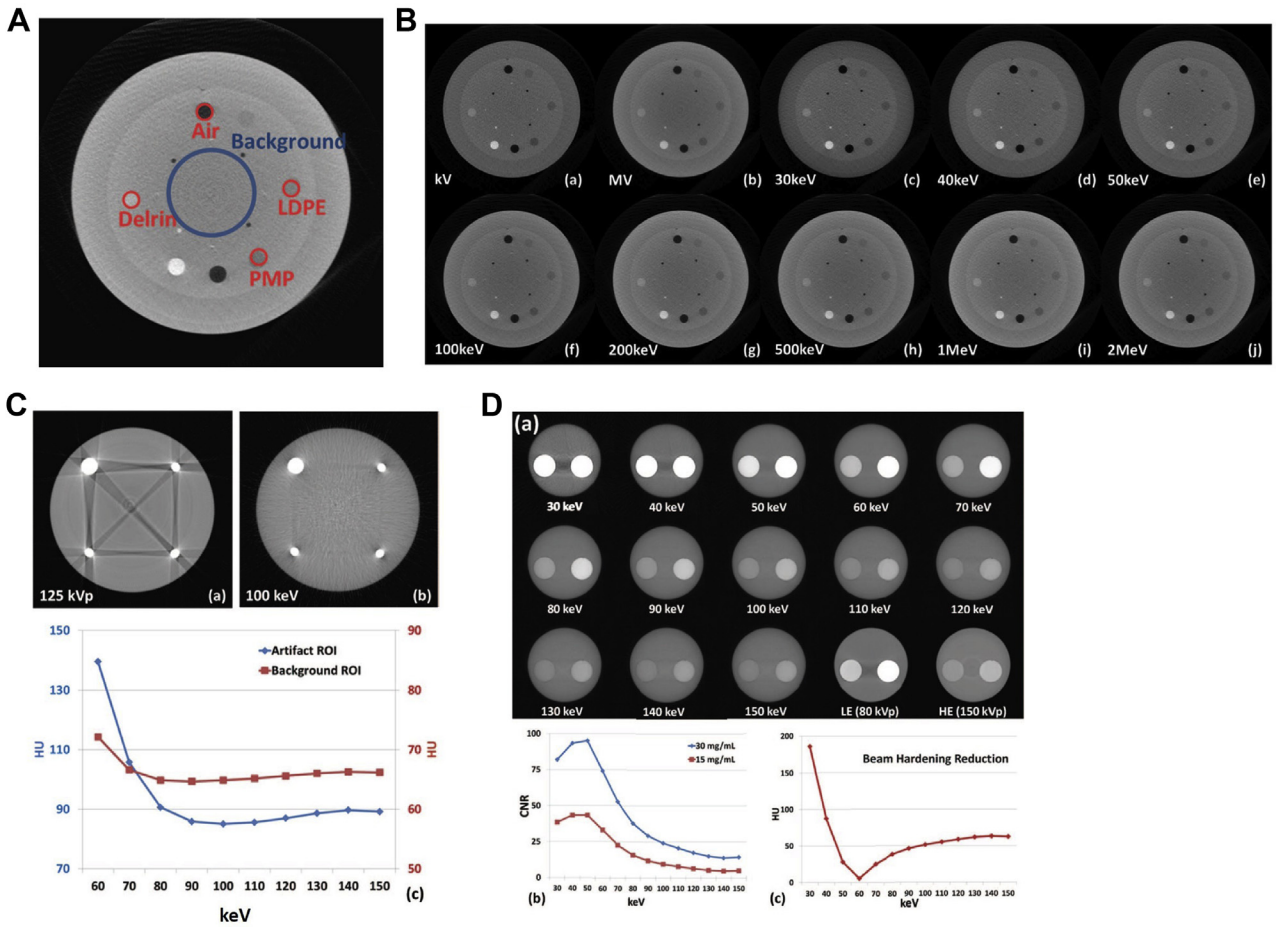

Figure 5 Technique for virtual monochromatic imaging on a benchtop cone beam computed tomography (CBCT) unit. (A) Region of interest (ROI) used for contrast-to-noise ratios (CNR) calculation. (B) CatPhan phantom axial slice reconstructions at kV, MV, and virtual monochromatic energies 30 keV through to 2 MeV. (C) Axial CBCTs of titanium-BB phantom at 125 kVp and virtual monochromatic 100 keV and corresponding HU of artifact and background. (D) Virtual monochromatic CBCTs of the water phantom containing 2 iodine concentrations at different keVs: 30 to 150 keV and LE (80 kVp) and HE (150 kVp). The corresponding CNR curves for the 2 iodine concentrations and the reduction in beam hardening artifact are shown on the curves beneath as a function of keV. (A-B) Adapted with permission from reference Li et al[34] (C-D) Adapted with permission from reference Li et al.[42]

existing literature for tumor visualization or localization in patients using DE-CBCT. To date, most investigations have been carried out using multimaterial phantoms with HU values in similar ranges to the tumors.[34,42,76] Figure 5B illustrates the visibility of inserts (illustrated in Fig 5A) of different HU values at different keV values.

Planar DE imaging can also have notable benefits with regard to tumor tracking,[77-79] especially in sites where motion is a significant concern, such as the lungs. During the course of treatment, the lung tumor position can vary by up to 2 cm owing to respiratory motion. This necessitates the treatment volumes to be expanded at the risk of healthy tissue being irradiated as well. Alternatively, the implantation of radio-opaque fiducial markers can be used for real-time motion tracking. This is an invasive process with risks, such as marker migration and pneumothorax. Markerless techniques such as fluoroscopy hold significant promise. However, overlying bones can often conceal the tumor borders hence creating a need for DE-fluoroscopy techniques.[79] A series of works have explored usage of DE-fluoroscopy images taken at a few different gantry angles.[78,80] An improvement was shown whereby the algorithm tracked the target in 99.9% of DE frames versus 90.7% of single energy (SE) images.[79] This is illustrated in Figure 6, where a lung tumor is shown to be more accurately tracked using DE. Also, in a recent report by Haytmyradov et al,[81] results were presented for markerless tumor tracking using fast-kV switching DE fluoroscopy. These results demonstrated an improvement in tracking accuracy specifically for small targets.[81] Also, preliminary results investigating DE-CBCT for lung tumor tracking indicated significant tracking improvement.[82] The algorithm tracked the tumor in 89.8% of the DE frames in comparison to 54.3% of the SE frames.

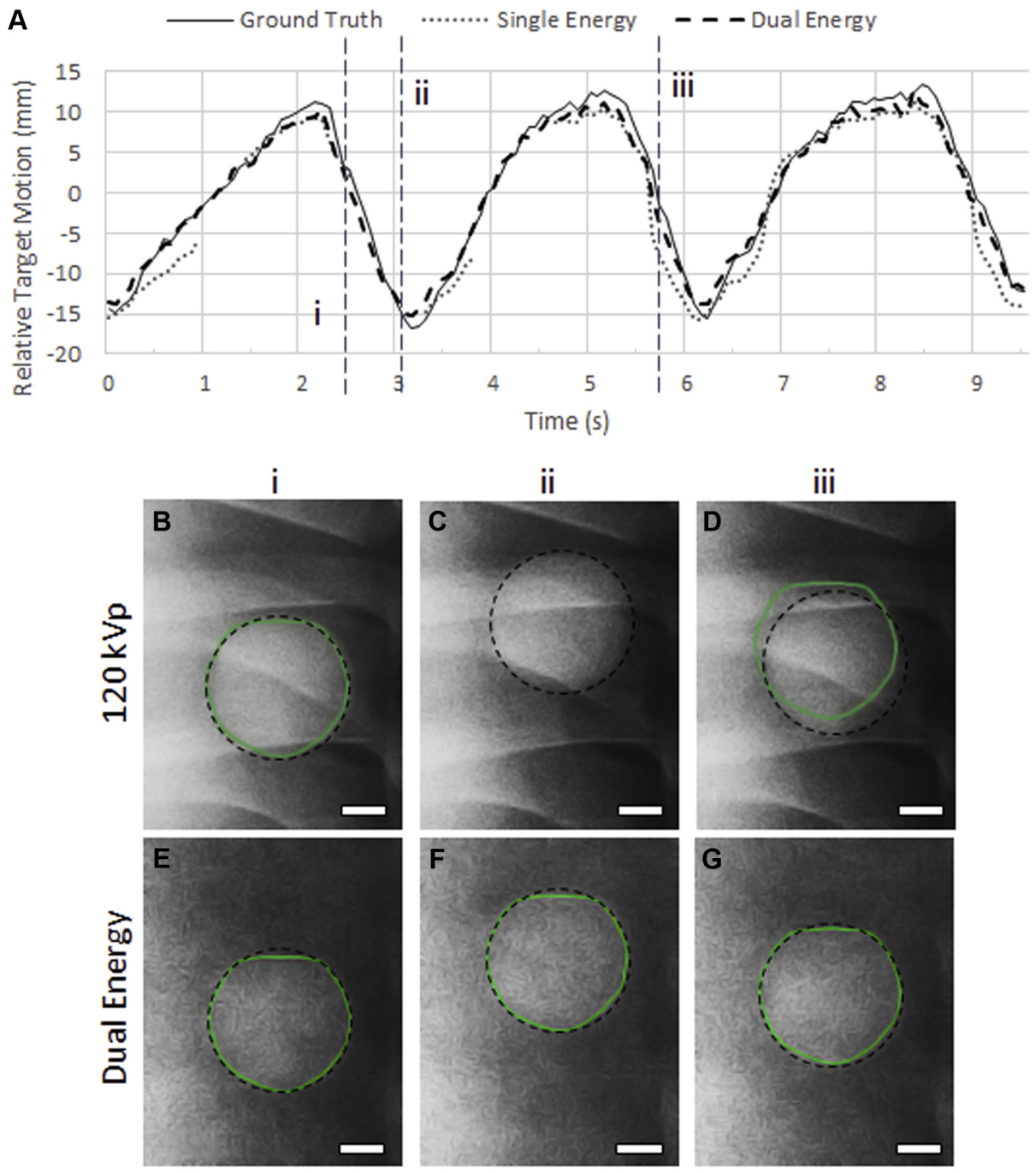

Figure 6 Example of DE fluoroscopy to improve lung tumor tracking. (A) The relative target motion is plotted against time where the y-coordinate of ground truth trace is compared with tracked y-coordinate obtained from SE and DE images. (B-D) SE frames from the locations (i, ii, iii) indicated in (A). (E-G) DE frames from the locations (i, ii, iii) indicated in (A). The tracked position of target is indicated by the highlighted contour and the ground-truth tumor position is indicated by the dashed outline (Bar = 1 cm). Better tracking is observed on using DE frames. Adapted with permission from reference Patel et al.[79]

Artifact reduction: metal artifacts and beam hardening

Two major artifacts seen in CBCT images are beam hardening (BH) and metal artifacts (in the presence of metallic structures). The underlying cause of metal artifacts is a combination of BH and photon starvation, which occurs when the x-ray beams pass through high-density structures and an insufficient number of photons reach the detector. Because the x-ray beams are fundamentally polychromatic in nature, different portions of the spectrum undergo different degrees of photon starvation

resulting in artifacts in the resultant image. Because DE imaging uses projection data that may have limited or inconsistent counts due to photon starvation, it cannot fully correct for photon starvation. BH occurs due to spectral shift which also results due to the polychromatic nature of x-ray beams. This can be partially mitigated through the use of monochromatic x-ray beams, which are only possible currently in synchrotron systems.[19,20] Alternatively, some CT-based[27,68] and few recent CBCT studies have investigated the potential use of VMPs to reduce BH and metal artifacts. In Figure 5C, a quantitative assessment of the reduction of the metal artifact arising from titanium ball bearing was done. Qualitatively a reduction in metal artifacts occurs using virtual monochromatic CBCT images. In Figure 5D, a quantification of the reduction of BH is illustrated. The BH artifact reduces steeply with increasing energy up to 60 keV and then gradually increases again. It should be noted that BH can be further decreased by combining DE imaging with conventional techniques to reduce BH artifacts.[83-85]

Improved Dose Calculations Using DE-CBCT

Brachytherapy

In the present section we discuss avenues in which DE-CBCT can potentially be used in the brachytherapy suite. It is worth noting that although there is no current clinical application of DE-CBCT in the brachytherapy suite, DE-CT has already been used for brachytherapy.[86-91] Standard techniques for brachytherapy applications using single energy CT (SECT) require a tissue segmentation step. In Remy et al,[90] it was found that DECT-based tissue segmentation can provide dose distributions of higher accuracy compared with SECT, in some situations such as under low noise conditions, for the organs at risk, and in case of calcifications surrounding the prostrate (94). In Remy et al,[90] a technique is presented using DE-CT for estimating parameters in an inhomogeneity correction factor that was previously proposed in AAPM TG-43[92] to account for tissue inhomogeneities, as emphasized in AAPM TG-186.[91] It should be noted, however, that the improvements in dose calculations using DE-CT in brachytherapy has primarily been presented for LE sources[87] such as I-125 and Pd-103.[86] HE sources, such as Ir-192, may see limited benefit from dual energy.

In the brachytherapy suite, as for planning, the use of verification CBCTs can be enhanced with more accurate dose calculations. Dose calculations in brachytherapy depend strongly on atomic numbers owing to the influence of photoelectric absorption at LE of photons emitted from the brachytherapy sources.[87,88,90] Accurate dose measurements require CT numbers (HU values), which is challenged in CBCT due to aforementioned artifacts. Several works have explored the suitability of CBCT images for dose calculations and pixel-based correction techniques have been proposed.[93,94] The dose accuracy can be improved by usage of patient-specific HU to density (D) curves.[95]

Intraoperative C-arms and O-arms are becoming increasingly used in brachytherapy suites for verification of seed or needle placement.[96] The image quality of such systems is negatively affected by BH[90] and scatter artifacts, which are also exacerbated by the implants themselves.[96] Applying DE-CBCT in these situations would reduce the effect of BH, which may increase implant localization accuracy. Furthermore, it would be advantageous to be able to calculate dose directly on the intraoperative images to verify that the loading pattern is adequate for tumor coverage. Owing to the LE penetration of the brachytherapy sources, accurate classification of tissue atomic number is required, as already demonstrated using DE-CT.[89] Although it remains to be commercially implemented, an effective implementation of DE-CBCT in the brachytherapy suite has the potential to facilitate intraoperative verification of brachytherapy dose distributions.

External beam radiation therapy or adaptive radiation therapy

Improvement in CBCT-based dose calculation could facilitate adaptive radiation therapy techniques. Current methods for using CBCT for adaptive radiation therapy include either deforming the planning CT to the daily CBCT or by assigning bulk-density to the CBCT. Both methods incur limitations, such as the accuracy of deformable image registration or assumptions made in bulk-density assignment. Ideally CT numbers could be inferred directly from the CBCT image because one could then convert CT numbers (HU) to electron density relative to water (ρ_e), which is required for dose calculation. Because HU[97] does not have a one-to-one correspondence with ρ_e owing to the dependence of HU on both effective atomic number (Z) and electron density (ρ_e), stoichiometric[97] techniques based on the HU-ρ_e relationship are limited in their ability to determine ρ_e, which results in reduced accuracy of the dose calculations. DE-CT provides the information needed for calculation of both Z and ρ_e hence enabling the usage of more precise stoichiometric techniques for conversion of HU to ρ_e.

A series of works in literature[97-100] have investigated usage of DE-CT for dose calculation. DE-CBCT techniques using image-domain reconstruction require accurate CT numbers for precise dose calculations. Adaptation of these techniques using DE-CBCT would necessitate either the development of projection-domain–based techniques or an improvement in the accuracy of CT number calculations from CBCT.

Proton and heavy ions in radiation therapy and verification

Proton therapy is receiving greater interest recently as shown by the 40% increase in the number of proton therapy centers in the past 3 to 4 years.[101,102]

Intensity modulated proton therapy is a technique ie, increasingly used and may confer some dosimetric advantages in particular for pediatric cases where the lack of exit dose minimizes the risk of long-term complications. However, intensity modulated proton therapy is technically demanding, and because of the position of the Bragg peak being sensitive to changes in radiologic path length, there is a risk of compromising target dose or overdosing organs-at-risk distal to the tumor.[62] It is well established in literature that DE-CT can improve the accuracy of stopping power ratios (SPRs). Most of the work[103,104] was based on image-domain techniques and rely on having accurate CT numbers. One of the works done with DE-CT showed equivalent performance of projection-domain technique to image-domain technique in DE-CT.[105] Hence for DE-CBCT, it would benefit to develop projection-domain techniques for this particular application as mass attenuation coefficients instead of CT numbers can be used for dose calculations.

Artifacts as a result of the dental fillings also add some uncertainty in terms of treatment planning.[101] Usage of techniques like VMPs described previously would be beneficial for artifacts reduction. Also, VMPs may assist in improving visualization. Motion can have deleterious effects on proton therapy dose distributions, and techniques such as DE-fluoroscopy executed on a CBCT system could potentially augment confidence in target localization throughout treatment.

Heavy ion (heavier than protons) offer some advantages compared with protons owing to the increased mass hence reduced scattering and sharper lateral dose deposition edges. The most prominent biologic advantage of heavy (eg, carbon ions over protons) is anticipated in tumors demonstrating low radiosensitivity[106] to photons. A number of prospective nonrandomized trials for various tumor sites such as nonsquamous cell head and neck tumors, prostate cancer, lung cancer, and locally advanced bone and soft tissue tumors have demonstrated the effectiveness of carbon ion radiation therapy.[106] However, heavy ion radiation therapy[103] is similarly affected by issues of range uncertainties, and dual-energy techniques (DE-CT/DE-CBCT) would aid in improving the accuracy of the SPRs[107] or water equivalent path lengths. In Hünemohr et al,[108] using pig tissue, it was demonstrated using the electron density images generated using DECT that both the noise levels and uncertainties in range calculation were smaller compared with corresponding values associated with SECT images. Thus, although clinical evidence of DECT for heavy ions is currently limited, preliminary literature indicates DECT's potential for uncertainty mitigation. Hence for onboard CBCT systems in heavy ion suites, dual-energy could contribute in the future to an online range uncertainty mitigation approach.

Radiomics

Radiomics[109-113] marks a shift from the traditional practice of studying medical images as pictures for the purposes of qualitative visual inspection toward an intricate process of extraction and quantification of data from these images. It involves high throughput extraction of features (such as shape, histogram, and texture) to capture the tumor heterogeneity. Additional models can be developed to improve the accuracy of prediction of clinical outcomes by combination with appropriate bioinformatics tools.[113] Aerts et al proposed a radiomics signature for predicting overall survival in lung cancer patients treated with radiation therapy.[109] Furthermore, radiomics-based approaches have shown promising results in adaptive radiation therapy for NSCLC.[114]

In radiation treatment, the CBCT images are collected before every fraction of treatment. Although the image quality of CBCT is degraded compared with CT owing to the artifacts caused by scatter and BH, these images present a source for tracking how the features evolve over the course of treatment,[115] which have potential to develop into biomarkers for early detection of tumor response. Furthermore, it has been shown in[116] that some radiomics features are sufficiently robust that they can be extracted from planning CT and CBCT interchangeably. It was shown by applying a previously developed CT-based radiomics signature[116] on 2-step corrected CBCT images, that prognostic information regarding overall survival can be determined from nonsmall cell lung carcinoma patient data before the start of treatment.

Furthermore, DE acquisition of the CBCT over the course of treatment could potentially provide more information. There would be images at 2 different energies, which can be further combined in different ways: linearly mixed, nonlinearly blended, material specific, and VMIs. The resultant database of the images can be used to provide specific information with unique features brought in by each category of images. For instance, VMIs would have reduced BH and metal artifacts.

Tumor characterization and response monitoring using nanoparticles

There has been an increasing amount of interest during the past decade in the use of gold nanoparticles (GNPs) as radiation sensitizers for radiation therapy applications.[117] GNPs have some favorable properties which render them amenable for this purpose: The high atomic number

(Z = 79) provides excellent radiation contrast. From biologic perspective, GNPs are quite well tolerated, and it has been concluded from observation that they can accumulate selectively in tumors and be excluded from healthy tissue.[117] Also different radiation types can be used with GNPs such as kV sources, MV sources, MeV electrons, heavily charged particles, and keV photons from brachytherapy.[117]

The degree of tumor angiogenesis can be accurately quantified using tumor blood volume and vascular permeability (VP). Tumor blood volume and VP are used as important predictors in cancer diagnosis, planning and treatment. In Clark et al,[118] DE micro-CT scanning technique using rapid kVp switching was used to decompose into 3-dimensional maps of iodine and gold. This allowed the simultaneous measurement of extravasated gold and intravascular iodine concentrations.[118] Simulations, calibration phantom-based testing and a mouse model genetically engineered to develop soft tissue sarcoma were used to test the success of the technique.[118] The work demonstrated the successful measurement of VP and FBV within tumors. The future applicability of this technique is promising for a variety of applications from tumor characterization to the monitoring of treatment response.[118]

Conclusions

DE-CBCT can potentially improve upon the limitations inherent in conventional CBCT by reducing artifacts and potentially improving lesion conspicuity with or without an exogenous contrast agent. DE-CBCT can be implemented in a number of ways, with modifications to the x-ray source, detector and acquisition workflow compared with conventional CBCT. Based on the existing work and an investigation of future applications, there is a clear potential for DE-CBCT technologies to be incorporated into radiation therapy. The applications of DE-CBCT include (but are not limited to): adaptive radiation therapy, brachytherapy, proton therapy, radiomics, and theranostics.

References

1. Jaffray DA, Siewerdsen JH, Wong JW, et al. Flat-panel cone-beam computed tomography for image-guided radiation therapy. *Int J Radiat Oncol Biol Phys*. 2002;53:1337-1349.
2. Purdie TG, Bissonnette JP, Franks K, et al. Cone-beam computed tomography for on-line image guidance of lung stereotactic radiotherapy: Localization, verification, and intrafraction tumor position. *Int J Radiat Oncol Biol Phys*. 2007;68:243-252.
3. Marchant TE, Joshi KD, Moore CJ, et al. Shading correction for cone-beam CT in radiotherapy: Validation of dose calculation accuracy using clinical images. *Proc. SPIE 10132, Medical Imaging 2017: Physics of Medical Imaging*. 9 March 2017:101320J.
4. Thing RS, Bernchou U, Hansen O, et al. Accuracy of dose calculation based on artefact corrected cone beam CT images of lung cancer patients. *Phys Imaging Radia. Oncol*. 2017;1:6-11.
5. Rührnschopf EP, Klingenbeck K. A general framework and review of scatter correction methods in x-ray cone-beam computerized tomography. Part 1: Scatter compensation approaches. *Med Phys*. 2011;38:4296-4311.
6. Xu Y, Bai T, Yan H, et al. A practical cone-beam CT scatter correction method with optimized Monte Carlo simulations for image-guided radiation therapy. *Phys Med Biol*. 2015;60:3567-3587.
7. Thing RS, Bernchou U, Mainegra-Hing E, et al. Patient-specific scatter correction in clinical cone beam computed tomography imaging made possible by the combination of Monte Carlo simulations and a ray tracing algorithm. *Acta Oncol (Madr)*. 2013;52:1477-1483.
8. McCollough CH, Leng S, Yu L, et al. Dual- and multi-energy CT: Principles, technical approaches, and clinical applications. *Radiology*. 2015;276:637-653.
9. Patino M, Prochowski A, Agrawal MD, et al. Material separation using dual-energy ct: Current and emerging applications. *RadioGraphics*. 2016;36:1087-1105.
10. Postma AA, Hofman PAM, Stadler AAR, et al. Dual-energy CT of the brain and intracranial vessels. *Am J Roentgenol*. 2012;199:26-33.
11. Potter CA, Sodickson AD. Dual-energy CT in emergency neuroimaging: Added value and novel applications. *RadioGraphics*. 2016;36:2186-2198.
12. Roele ED, Timmer VCML, Vaassen LAA, et al. Dual-energy CT in head and neck imaging. *Curr Radiol Rep*. 2017:5-19.
13. Forghani R, De Man B, Gupta R. Dual-energy computed tomography: Physical principles, approaches to scanning, usage, and implementation: Part 2. *Neuroimaging Clin N Am*. 2017;27:385-400.
14. Van Elmpt W, Landry G, Das M, et al. Dual energy CT in radiotherapy: Current applications and future outlook. *Radiother Oncol*. 2016;119:137-144.
15. Jacobson B. Dichromatic absorption radiography. *Dichromography. Acta Radiol*. 1953;39:437-452.
16. Mistretta CA, Kelcz F. Compensation for patient thickness variations in differential x-ray transmission imaging. *US Patent*. 1974.
17. Alvarez RE, MacOvski A. Energy-selective reconstructions in x-ray computerised tomography. *Phys Med Biol*. 1976;21:733-744.
18. Chotas HG, Dobbins JT, Ravin CE. Principles of digital radiography with large-area, electronically readable detectors: A review of the basics. *Radiology*. 1999;210:595-599.
19. Torikoshi M, Tsunoo T, Sasaki M, et al. Electron density measurement with dual-energy x-ray CT using synchrotron radiation. *Phys Med Biol*. 2003;48:673-685.
20. Tsunoo T, Torikoshi M, Ohno Y, et al. Measurement of electron density in dual-energy x-ray CT with monochromatic x rays and evaluation of its accuracy. *Med Phys*. 2008;35:4924-4932.
21. Richard S. *Optimization of imaging performance and conspicuity in dual-energy x-ray radiography [thesis]*. University of Toronto; 2008.
22. Johnson TRC. Dual-energy CT: General principles. *Am J Roentgenol*. 2012;199:S3-S8.
23. Shikhaliev PM. Photon counting spectral CT: Improved material decomposition with K-edge-filtered x-rays. *Phys Med Biol*. 2012;57:1595-1615.
24. Roessl E, Proksa R. K-edge imaging in x-ray computed tomography using multi-bin photon counting detectors. *Phys Med Biol*. 2007;52:4679-4696.
25. Johnson TRC, Kalender WA. Physical background of CT technologies. In: *Dual Energy CT in Clinical Practice*. Berlin Heidelberg: Springer-Verlag; 2011:3-9.

26. Primak AN, Ramirez Giraldo JC, Liu X, et al. Improved dual-energy material discrimination for dual-source CT by means of additional spectral filtration. *Med Phys*. 2009;36:1359-1369.
27. Yu L, Christner JA, Leng S, et al. Virtual monochromatic imaging in dual-source dual-energy CT: Radiation dose and image quality. *Med Phys*. 2011;38:6371-6379.
28. Krauss B, Schmidt B, Flohr T. Dual source CT. In: *Dual Energy CT in Clinical Practice*. Berlin Heidelberg: Springer-Verlag; 2011: 11-20.
29. Giles W, Bowsher J, Li H, et al. Interleaved acquisition for cross scatter avoidance in dual cone-beam CT. *Med Phys*. 2012;39:7719-7728.
30. Ren L, Chen Y, Zhang Y, et al. Scatter reduction and correction for dual-source cone-beam CT using prepatient grids. *Technol Cancer Res Treat*. 2015;15:416-427.
31. Petersilka M, Stierstorfer K, Bruder H, et al. Strategies for scatter correction in dual source CT. *Med Phys*. 2010;37:5971-5992.
32. Li H, Giles W, Bowsher J, et al. A dual cone-beam CT system for image guided radiotherapy: Initial performance characterization. *Med Phys*. 2013;40:021912:1-11.
33. Li H, Yin F-F, Bowsher J, et al. *Investigation of Imaging Capabilities for Dual Cone-Beam Computed Tomography. Phd. Thesis*. Duke University; 2013.
34. Li H, Liu B, Yin FF. Generation of virtual monochromatic CBCT from dual kV/MV beam projections. *Med Phys*. 2013;40:121910:1-121910:9.
35. Blessing M, Stsepankou D, Wertz H, et al. Breath-hold target localization with simultaneous kilovoltage/megavoltage cone-beam computed tomography and fast reconstruction. *Int J Radiat Oncol Biol Phys*. 2010;78:1219-1226.
36. Wertz H, Stsepankou D, Blessing M, et al. Fast kilovoltage/megavoltage (kVMV) breathhold cone-beam CT for image-guided radiotherapy of lung cancer. *Phys Med Biol*. 2010; 55:4203-4217.
37. Zbijewski W, Sisniega A, Stayman JW, et al. Dual-energy imaging of bone marrow edema on a dedicated multi-source cone-beam CT system for the extremities. *Proc SPIE, Medical Imaging 2015: Physics of Medical Imaging*. 18 March 2015; 9412:94120V.
38. Goodsitt MM, Christodoulou EG, Larson SC. Accuracies of the synthesized monochromatic CT numbers and effective atomic numbers obtained with a rapid kVp switching dual energy CT scanner. *Med Phys*. 2011;38:2222-2232.
39. Chandra N, Langan DA. Gemstone detector: Dual energy imaging via fast kVp switching. In: *Dual Energy CT in Clinical Practice*. Berlin Heidelberg: Springer-Verlag; 2011:5-41.
40. So A, Lee TY, Imai Y, et al. Quantitative myocardial perfusion imaging using rapid kVp switch dual-energy CT: Preliminary experience. *J Cardiovasc Comput Tomogr*. 2011;5:430-442.
41. Min J, Lee T, Kim K-W, et al. Low-dose dual-energy cone-beam CT using a total-variation minimization algorithm. Proc. SPIE, Medical Imaging 2011: Physics of Medical Imaging.
42. Li H, Giles W, Ren L, et al. Implementation of dual-energy technique for virtual monochromatic and linearly mixed CBCTs. *Med Phys*. 2012;39:6056-6064.
43. Zbijewski W, Gang GJ, Xu J, et al. Dual-energy cone-beam CT with a flat-panel detector: Effect of reconstruction algorithm on material classification. *Med Phys*. 2014;41:1-15.
44. Zbijewski W, Qian C, Tilley S, et al. Quantitative assessment of bone and joint health on a dedicated extremities cone-beam CT system. *Int J Comput Assist Radiol Surg*. 2015;10:1-5.
45. Granton PV, Pollmann SI, Ford NL, et al. Implementation of dual- and triple-energy cone-beam micro-CT for postreconstruction material decomposition. *Med Phys*. 2008;35:5030-5042.
46. Vlassenbroek A. Dual layer CT. In: *Dual Energy CT in Clinical Practice*. Berlin Heidelberg: Springer-Verlag; 2011:21-34.
47. Han JC, Kim HK, Kim DW, et al. Single-shot dual-energy x-ray imaging with a flat-panel sandwich detector for preclinical imaging. *Curr Appl Phys*. 2014;14:1734-1742.
48. Alvarez RE, Seibert JA, Thompson SK. Comparison of dual energy detector system performance. *Med Phys*. 2004;31:556-565.
49. Hu YH, Rottmann J, Fueglistaller R, et al. Leveraging multi-layer imager detector design to improve low-dose performance for megavoltage cone-beam computed tomography. *Phys Med Biol*. 2018;63:035022.
50. Hu YH, Fueglistaller R, Myronakis M, et al. Physics considerations in MV-CBCT multi-layer imager design. *Phys Med Biol*. 2018;63:125016.
51. Fueglistaller R, Shedlock D, Myronakis M, et al. Characterizing a novel scintillating glass for application to megavoltage cone-beam computed tomography. *Med Phys*. 2018;46:1323-1330.
52. Rottmann J, Berbeco RI, Wang A, et al. A novel multilayer MV imager computational model for component optimization. *Med Phys*. 2017;44:4213-4222.
53. Myronakis M, Fueglistaller R, Rottmann J, et al. Spectral imaging using clinical megavoltage beams and a novel multi-layer imager. *Phys Med Biol*. 2017;62:9127-9139.
54. Myronakis M, Hu YH, Fueglistaller R, et al. Multi-layer imager design for mega-voltage spectral imaging. *Phys Med Biol*. 2018;63: 105002.
55. Chen H, Morf D, Rottmann J, et al. Super-resolution imaging in a multiple layer EPID. *Biomed Phys Eng Express*. 2017;3:025004.
56. Star-Lack J, Morf D, Yip S, et al. TH-EF-BRB-02: Combination of multiple EPID imager layers improves image quality and tracking performance of low contrast objects. *Med Phys*. 2015;42, 3742-3742.
57. Rottmann J, Morf D, Fueglistaller R, et al. A novel EPID design for enhanced contrast and detective quantum efficiency. *Phys Med Biol*. 2016;61:6297-6306.
58. Taguchi K, Iwanczyk JS. Vision 20/20: Single photon counting x-ray detectors in medical imaging. *Med Phys*. 2013;40:100901:1-100901:19.
59. Ahmad M, Fahrig R, Pung L, et al. Assessment of a photon-counting detector for a dual-energy C-arm angiographic system. *Med Phys*. 2017;44:5938-5948.
60. Xu J, Zbijewski W, Gang G, et al. Cascaded systems analysis of photon counting detectors. *Med Phys*. 2014;101907:1-15.
61. Wang X, Meier D, Taguchi K, et al. Material separation in x-ray CT with energy resolved photon-counting detectors. *Med Phys*. 2011;38:1534-1546.
62. Wang X, Meier D, Mikkelsen S, et al. MicroCT with energy-resolved photon-counting detectors. *Phys Med Biol*. 2011;56: 2791-2816.
63. Schlomka JP, Roessl E, Dorscheid R, et al. Experimental feasibility of multi-energy photon-counting K-edge imaging in pre-clinical computed tomography. *Phys Med Biol*. 2008;53:4031-4047.
64. Johnson TRC, Krauß B, Sedlmair M, et al. Material differentiation by dual energy CT: Initial experience. *Eur Radiol*. 2007;17:1510-1517.
65. Tran DN, Straka M, Roos JE, et al. Dual-energy CT discrimination of iodine and calcium. experimental results and implications for lower extremity CT angiography. *Acad Radiol*. 2009;16:160-171.
66. Shkumat NA, Siewerdsen JH, Dhanantwari AC, et al. Optimization of image acquisition techniques for dual-energy imaging of the chest. *Med Phys*. 2007;34:3904.
67. Gang GJ, Zbijewski W, Webster Stayman J, et al. Cascaded systems analysis of noise and detectability in dual-energy cone-beam CT. *Med Phys*. 2012;39:5145-5156.
68. Kuchenbecker S, Faby S, Sawall S, et al. Dual energy CT: How well can pseudo-monochromatic imaging reduce metal artifacts? *Med Phys*. 2015;42:1023-1036.
69. Cardinal HN, Fenster A. Accurate method for direct dual energy calibration and decomposition. *Med Phys*. 1990;17:327-341.

70. Gang GJ, Varon CA, Kashani H, et al. Multiscale deformable registration for dual-energy x-ray imaging. *Med Phys*. 2009;36:351-363.
71. Fan Q, Lu B, Park JC, et al. Image-domain shading correction for cone-beam CT without prior patient information. *J Appl Clin Med Phys*. 2015;16:65-75.
72. Holmes DR, Fletcher JG, Apel A, et al. Evaluation of non-linear blending in dual-energy computed tomography. *Eur J Radiol*. 2008;68:409-413.
73. Ascenti G, Krauss B, Mazziotti S, et al. Dual-energy computed tomography (DECT) in renal masses. Nonlinear versus linear blending. *Acad Radiol*. 2012;19:1186-1193.
74. Forghani R, Mukherji SK. Advanced dual-energy CT applications for the evaluation of the soft tissues of the neck. *Clin Radiol*. 2018;73:70-80.
75. De Cecco CN, Laghi A, Joseph Schoepf U, et al. *Dual energy CT in oncology*. Switzerland: Springer International Publishing; 2015.
76. Sajja S, Hashemi CM, Huynh C, et al. Investigation of calibration-based projection domain dual energy decomposition CBCT technique for brain radiotherapy applications. *Proc SPIE, Medical Imaging 2019: Physics of Medical Imaging*. 1 March 2019;10948:10948A.
77. Hoggarth MA, Luce J, Syeda F, et al. Dual energy imaging using a clinical on-board imaging system. *Phys Med Biol*. 2013;58:4331-4340.
78. Sherertz T, Hoggarth M, Luce J, et al. Prospective evaluation of dual-energy imaging in patients undergoing image guided radiation therapy for lung cancer: Initial clinical results. *Int J Radiat Oncol Biol Phys*. 2014;89:525-531.
79. Patel R, Panfil J, Campana M, et al. Markerless motion tracking of lung tumors using dual-energy fluoroscopy. *Med Phys*. 2014;42:254-262.
80. Dhont J, Poels K, Verellen D, et al. Feasibility of markerless tumor tracking by sequential dual-energy fluoroscopy on a clinical tumor tracking system. *IFMBE Proc*. 2015;51:591-594.
81. Haytmyradov M, Mostafavi H, Wang A, et al. Markerless tumor tracking using Fast-kV switching dual energy fluoroscopy on a benchtop system. *Med Phys*. 2019;46:3235-3244.
82. Panfil J, Patel R, Surucu M, et al. WE-G-BRF-05: Feasibility of markerless motion tracking using dual energy cone beam computed tomography (DE-CBCT) projections. *Med Phys*. 2014;41:522.
83. Li Y, Garrett J, Chen G. Reduction of beam hardening artifacts in cone-beam CT imaging via SMART-RECON algorithm. *Proc of SPIE Opt Eng*. 2016:9783.
84. Dang H, Stayman JW, Sisniega A, et al. Statistical reconstruction for cone-beam CT with a post-artifact-correction noise model: Application to high-quality head imaging. *Phys Med Biol*. 2015;60:6153-6175.
85. Sisniega A, Zbijewski W, Xu J, et al. High-fidelity artifact correction for cone-beam CT imaging of the brain. *Phys Med Biol*. 2015;60:1415-1439.
86. Landry G, Granton PV, Reniers B, et al. Simulation study on potential accuracy gains from dual energy CT tissue segmentation for low-energy brachytherapy Monte Carlo dose calculations. *Phys Med Biol*. 2011;56:6257-6278.
87. Mashouf S, Lechtman E, Lai P, et al. Dose heterogeneity correction for low-energy brachytherapy sources using dual-energy CT images. *Phys Med Biol*. 2014;59:5305-5316.
88. Malusek A, Karlsson M, Magnusson M, et al. The potential of dual-energy computed tomography for quantitative decomposition of soft tissues to water, protein and lipid in brachytherapy. *Phys Med Biol*. 2013;58:771-785.
89. Landry G, Gaudreault M, van Elmpt W, et al. Improved dose calculation accuracy for low energy brachytherapy by optimizing dual energy CT imaging protocols for noise reduction using sinogram affirmed iterative reconstruction. *Z Med Phys*. 2016;26:75-87.
90. Remy C, Lalonde A, Béliveau-Nadeau D, et al. Dosimetric impact of dual-energy CT tissue segmentation for low-energy prostate brachytherapy: A Monte Carlo study. *Phys Med Biol*. 2018;63:025013.
91. Davis SD, Rivard MJ, Thomson RM, et al. Report of the Task Group 186 on model-based dose calculation methods in brachytherapy beyond the TG-43 formalism: Current status. *Med Phys*. 2012;39:6208-6236.
92. Rivard MJ, Coursey BM, DeWerd LA, et al. Update of AAPM task group No. 43 report: A revised AAPM protocol for brachytherapy dose calculations. *Med Phys*. 2004;31:633-674.
93. Morin O, Chen J, Aubin M, et al. Dose calculation using megavoltage cone-beam CT. *Int J Radiat Oncol Biol Phys*. 2007;67:1201-1210.
94. van Zijtveld M, Dirkx M, Heijmen B. Correction of conebeam CT values using a planning CT for derivation of the "dose of the day. *Radiother Oncol*. 2007;85:195-200.
95. Richter A, Hu Q, Steglich D, et al. Investigation of the usability of conebeam CT data sets for dose calculation. *Radiat Oncol*. 2008;3:1-13.
96. Polo A, Salembier C, Venselaar J, et al. Review of intraoperative imaging and planning techniques in permanent seed prostate brachytherapy. *Radiother Oncol*. 2010;94:12-23.
97. Saito M. Potential of dual-energy subtraction for converting CT numbers to electron density based on a single linear relationship. *Med Phys*. 2012;39:2021-2030.
98. Tsukihara M, Noto Y, Hayakawa T, et al. Conversion of the energy-subtracted CT number to electron density based on a single linear relationship: An experimental verification using a clinical dual-source CT scanner. *Phys Med Biol*. 2013;58:N135-N144.
99. Saito M, Tsukihara M. Technical note: Exploring the limit for the conversion of energy-subtracted CT number to electron density for high-atomic-number materials. *Med Phys*. 2014;41:071701-071701:6.
100. Saito M, Sagara S. A simple formulation for deriving effective atomic numbers via electron density calibration from dual-energy CT data in the human body. *Med Phys*. 2017;44:2293-2303.
101. Mohan R, Das IJ, Ling CC. Empowering intensity modulated proton therapy through physics and technology: An overview. *Int J Radiat Oncol Biol Phys*. 2017;99:304-316.
102. Zietman AL. Particle therapy at the "tipping point": An introduction to the red journal's special edition. *Int J Radiat Oncol Biol Phys*. 2016;95:1-3.
103. Wohlfahrt P, Möhler C, Richter C, et al. Evaluation of stopping-power prediction by dual- and single-energy computed tomography in an anthropomorphic ground-truth phantom. *Int J Radiat Oncol Biol Phys*. 2018;100:244-253.
104. Hudobivnik N, Schwarz F, Johnson T, et al. Comparison of proton therapy treatment planning for head tumors with a pencil beam algorithm on dual and single energy CT images comparison of proton therapy treatment planning for head tumors with a pencil beam algorithm on dual and single energy CT imag. *Med Phys*. 2016;495:495-504.
105. Vilches-Freixas G, Taasti VT, Muren LP, et al. Comparison of projection- and image-based methods for proton stopping power estimation using dual energy CT. *Phys Imaging Radiat Oncol*. 2017;3:28-36.
106. Schulz-Ertner D, Tsujii H. Particle radiation therapy using proton and heavier ion beams. *J Clin Oncol*. 2007;25:953-964.
107. Li B, Lee HC, Duan X, et al. Comprehensive analysis of proton range uncertainties related to stopping-power-ratio estimation using dual-energy CT imaging. *Phys Med Biol*. 2017;62:7056-7074.
108. Hünemohr N, Krauss B, Dinkel J, et al. Ion range estimation by using dual energy computed tomography. *Z Med Phys*. 2013;23:300-313.

109. Aerts HJWL, Velazquez ER, Leijenaar RTH, et al. Decoding tumour phenotype by noninvasive imaging using a quantitative radiomics approach. *Nat Commun*. 2014;5:4006,1-8.
110. Parmar C, Grossmann P, Bussink J, et al. Machine learning methods for quantitative radiomic biomarkers. *Sci Rep*. 2015; 5:1-11.
111. Aerts HJWL. The potential of radiomic-based phenotyping in precisionmedicine a review. *JAMA Oncol*. 2016;2:1636-1642.
112. Lambin P, Rios-Velazquez E, Leijenaar R, et al. Radiomics: Extracting more information from medical images using advanced feature analysis. *Eur J Cancer*. 2012;48:441-446.
113. Wu J, Tha KK, Xing L, et al. Radiomics and radiogenomics for precision radiotherapy. *J Radiat Res*. 2018;59:i25-i31.
114. Ramella S, Id MF, Id CG, et al. A radiomic approach for adaptive radiotherapy in non-small cell lung cancer patients. *PLoS One*. 2018:1-14.
115. Fave X, MacKin D, Yang J, et al. Can radiomics features be reproducibly measured from CBCT images for patients with non-small cell lung cancer? *Med Phys*. 2015;42:6784-6797.
116. van Timmeren JE, Leijenaar RTH, van Elmpt W, et al. Survival prediction of non-small cell lung cancer patients using radiomics analyses of cone-beam CT images. *Radiother Oncol*. 2017;123: 363-369.
117. Schuemann J, Berbeco R, Chithrani DB, et al. Roadmap to clinical use of gold nanoparticles for radiation sensitization. *Int J Radiat Oncol Biol Phys*. 2016;94:189-205.
118. Clark DP, Ghaghada K, Moding EJ, et al. In vivo characterization of tumor vasculature using iodine and gold nanoparticles and dual energy micro-CT. *Phys Med Biol*. 2013;58:1683-1704.
119. Willemink MJ, Persson M, Pourmorteza A, et al. Photon-counting CT: Technical principles and clinical prospects. *Radiology*. 2018; 289:293-312.